NISTIR 6427

THE FLUID DYNAMICS OF FIRE WHIRLS - - AN INVISCID MODEL

Francine Battaglia, Ronald G. Rehm and Howard R. Baum

Building and Fire Research Laboratory
Gaithersburg, Maryland 20899

United States Department of Commerce
Technology Administration
National Institute of Standards and Technology

NISTIR 6427

THE FLUID DYNAMICS OF FIRE WHIRLS - - AN INVISCID MODEL

Ronald G. Rehm

February 2000
Building and Fire Research Laboratory
National Institute of Standards and Technology
Gaithersburg, MD 20899

U.S. DEPARTMENT OF COMMERCE
William M. Daley, Secretary
TECHNOLOGY ADMINISTRATION
Dr. Cheryl L. Shavers, Under Secretary of Commerce for Technology
NATIONAL INSTITUTE OF STANDARDS AND TECHNOLOGY
Raymond G. Kammer, Director

TABLE OF CONTENTS

The Fluid Dynamics of Fire Whirls – An Inviscid Model

Francine Battaglia, Ronald G. Rehm and Howard R. Baum
National Institute of Standards and Technology
Building and Fire Research Laboratory
100 Bureau Dr. Stop 8640
Gaithersburg, MD 20899-8640

Abstract

Whirling fire plumes are known to increase the danger of naturally occurring or post-disaster fires. In order for a fire whirl to exist, there must be an organized source of angular momentum to produce the large swirl velocities as air is entrained into the fire plume. These vorticity-driven fires occur over a large range of length and velocity scales, and significantly alter the entrainment and combustion dynamics. A new model that incorporates angular rotation and neglects dissipation is derived for a buoyant plume; the result is a form of the steady state Euler equations. Included is a general solution for large density and temperature variations. Results that identify the mechanisms and their effects on the creation of a fire whirl are presented.

I. Introduction

Fire whirls are a rare but potentially catastrophic form of fire. They require an organized source of angular momentum to produce the large swirl velocities observed as air is entrained into the fire plume. A fire whirl can be generated on laboratory scales or can occur naturally on much larger length scales where atmospheric variations might influence their structure. We will be concerned here only with laboratory-scale fire whirls.

One of the earliest studies to systematically examine the fire whirl phenomena experimentally was carried out by Emmons and Ying [1]. They produced a fire whirl by burning a pool of acetone within a rotating cylindrical screen. The most striking characteristic of the experiments is that a very tall slender column of burning gases can be produced above the pool when the screen is rotated. Figure 1 shows the difference between a non-swirling fire (left) and swirling fire (right) that was produced by the experiments of Emmons [2]. Such observations contrast with all other fire plume experiments without angular momentum where the plume above the pool fire grows radially as ambient fluid is entrained. These observations are even more startling because the height of the luminous region (the flame) can extend to 30 pool diameters or more.

The model proposed in this paper is motivated by these observations: we wish to understand the mechanism by which such a long, slender cylindrical flame could arise. The most important physical phenomena involved in the fire whirl are the buoyancy generated by the

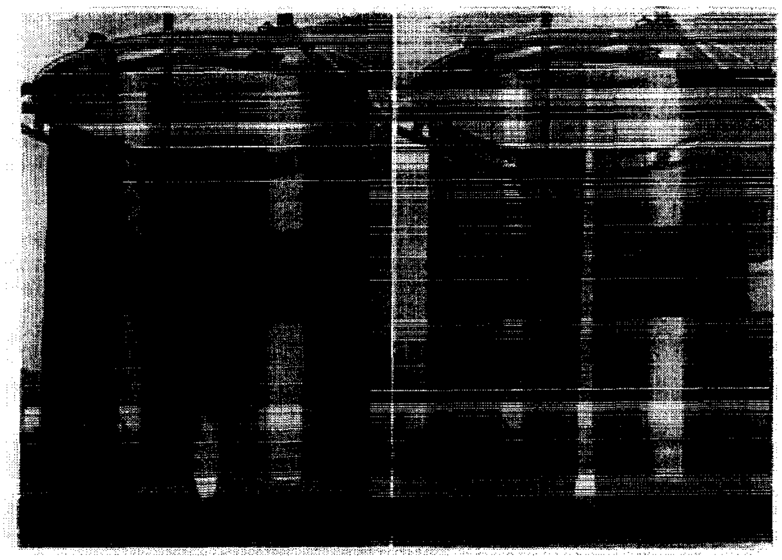

FIGURE 1: Pool fire experiments of Emmons [2] for a flame of acetone burning in a 10 cm (4 in.) diameter can. Left: 46 cm (1.5 ft) high flame without screen rotation. Right: 4.6 m (15 ft) high flame with screen (2.4 m (8 ft) diameter, 3.0 m (10 ft) high) rotating at 4 rpm.

gas-phase combustion and the externally imposed angular rotation. While the experiments [1] showed that the plume could undergo precession and while instabilities could also arise, often the long slender plume stood erect for long periods of time. This behavior of the flame implies that mixing of ambient fluid is very inhibited, that dissipation is small and that the columnar flame is nearly time independent. Therefore, in the model we assume a steady state in which angular rotation and buoyancy are the key components, but dissipation is ignored. We leave the mathematical description of dissipation and combustion for later analyses.

There are other studies that have also attempted to explain the dynamical behavior of swirl interacting with a buoyant plume. A review by Morton [3] describes the underlying mechanisms which produce and sustain a fire whirl. A mathematical description of a swirling buoyant plume arising from a point source of heat was presented by Thomas and Takhar [4]. Their analyses included cases for which circulation decays to zero outside of the plume or remains a finite constant. While the analysis of these cases showed qualitatively different behavior, neither would explain the observed plume dynamics found by Emmons and Ying.

Full-scale experiments might appear to be the most obvious way to study fire whirls. However, studies of this kind are limited by concerns for safety, economy, control and feasibility. Scale modeling is one approach to investigate fires under more manageable conditions by conducting small-scale experiments [5, 6, 7]. The literature includes reports by Williams [5] which address the importance of scaling mass fires. Soma and Saito [6] have been successful in developing scaling laws to model prototype fire whirls. An extensive review on the progress of experimental investigations in fire spread scenarios has been reported by Hirano and Saito [7].

Recently, an experimental study of swirling fires was presented by Satoh and Yang [8]. They followed these experiments with a numerical investigation to substantiate their observations [9]. The fire took place in a rectangular compartment with vertical asymmetric inlets to generate a swirling motion. The model predictions gave qualitatively similar results to those observed in experiments. However, the simulations were relatively low resolution and did not include a combustion model.

Other studies examined swirling [10, 11] and whirling [12] non-premixed flames. The fire whirl experiment of Emmons and Ying [1] was extended by Chigier et al. [10], replacing the liquid pool with a turbulent jet diffusion flame. The experiments yielded increased flame lengths of the fuel jet with either increasing rotation, increasing flow rates, or both. Tangirala and Driscoll [11] studied a fuel jet surrounded by coaxial swirling air and found that increasing swirl decreased the jet-like flame to a short intense flame, with improved stability, rapid mixing, and increased temperatures. Increasing fuel jet momentum produced a more jet-like flame. According to Gabler et al. [12], whirling flames differ from swirling flames: swirling combines both axial and azimuthal motions of a flow, whereas whirling flames are produced purely by azimuthal motion. We will not make such a distinction in this paper, using the words swirl and whirl interchangably. It appears that jet flames [10, 11, 12] can behave differently depending on how the rotation is applied to the flowfield. Flame lengths seem to decrease when rotation is imparted to the jet, but increase when rotation is imparted to the environment.

In general, fire whirls have not been adequately studied either theoretically or experimentally, and so the impact of swirl on the fluid dynamics and combustion process is not fully understood. Recently, the authors numerically investigated swirling fire plumes to analyze how swirl alters the plume dynamics and combustion [13]. The methodology was based on direct solution of the large scales and sub-grid scale approximations for the dynamic viscosity and heat release. The approach taken for swirling fires was to impose circulation while maintaining a constant heat release rate. It was shown that increasing circulation has a strong influence on the shape of the fire plume, and the whirling fires increased in length and constricted radially, consistent with previous literature. However, the resolution limits imposed by present computers restrict the range of dynamically active length scales that can be included. The present paper is aimed at exploring a model in which this limitation is removed.

This paper is laid out as follows. Section II.A. begins with the formulation of the Boussinesq model. Section II.B. continues with the formulation by relaxing the Boussinesq constraint and incorporating large density variations. The nondimensional form of the governing equations and the boundary conditions are described at the end of Section II.. Section III. is a presentation and discussion of the results for a buoyant plume with and without swirl. The section begins with a description of how the plume changes when subjected to different levels of circulation. The differences in plume development using the Boussinesq and non-Boussinesq model are contrasted. The contribution of this paper is the presentation of a tractable model formulation and solution of the inviscid equations of motion which allows the systematic analysis of the interaction of swirl and buoyancy. The summary will address the advantages and limitations of the simulations to establish goals of future work.

II. Methodology

A. Boussinesq Fluid

A fire whirl can be regarded as a rotational flow in which combustion drives convection through buoyancy. A simplified model of this convection is one where externally imposed swirl (circulation) and buoyancy interact. Assume that the flow is axisymmetric, steady and inviscid. The steady state Euler equations for a perfect gas in the low Mach number limit result in a tractable model with minimal complexity. The complete set of equations are [14]

$$\nabla \cdot \rho \mathbf{u} = 0 \tag{1}$$

$$\rho\left(\frac{1}{2}\nabla|\mathbf{u}|^2 - \mathbf{u}\times\boldsymbol{\omega}\right) + \nabla p - \rho\mathbf{g} = 0 \tag{2}$$

$$\mathbf{u}\cdot\nabla T = 0 \tag{3}$$

$$p_0 = \rho R T\ . \tag{4}$$

The fluid variables are density ρ, total velocity $\mathbf{u}$, vorticity $\boldsymbol{\omega} \equiv \nabla \times \mathbf{u}$, the dynamic pressure p, the ambient pressure p_0, gravity $\mathbf{g} \equiv -g\mathbf{i_z}$, temperature T and the gas constant R.

For the Boussinesq model, the density is replaced by the ambient density ρ_0 in the inertial terms of the momentum equation (Eq. (2)) and density variations from ambient are small. Note that the more general non-Boussinesq problem can be reduced to that of the Boussinesq model, and will be discussed in section B. With the Boussinesq approximation, the head $\mathcal{H}$ is

$$\mathcal{H} \equiv \frac{p - p_0}{\rho_0} + \frac{1}{2}|\mathbf{u}|^2 + gz\ . \tag{5}$$

Then, the conservation equations of mass, momentum and energy become

$$\nabla \cdot \mathbf{u} = 0 \tag{6}$$

$$-\mathbf{u}\times\boldsymbol{\omega}+\nabla\mathcal{H}+\left(\frac{T-T_0}{T_0}\right)\mathbf{g}=0 \tag{7}$$

$$\mathbf{u}\cdot\nabla\left(\frac{T-T_0}{T_0}\right)=0\,. \tag{8}$$

The continuity equation is satisfied by a stream function ψ in cylindrical coordinates (r,θ,z) with velocity components (u,v,w):

$$ru=-\frac{\partial\psi}{\partial z}\,; \qquad\qquad rw=\frac{\partial\psi}{\partial r}\,. \tag{9}$$

The energy equation can then be written, using the notation $\Theta\equiv(T-T_0)/T_0$:

$$\frac{\partial(\Theta,\psi)}{\partial(z,r)}=0\,.$$

This equation has the integral $\Theta=\Theta_0(\psi)$.

Similarly, there are integrals of the momentum equations. Define the circulation $\Gamma\equiv 2\pi rv$. Then, the azimuthal (swirl) equation becomes

$$\frac{\partial(\Gamma,\psi)}{\partial(z,r)}=0$$

with integral $\Gamma=\Gamma_0(\psi)$. The radial and axial components of the momentum equations, after taking the scalar product with $\mathbf{u}$ becomes

$$\frac{\partial(\mathcal{H},\psi)}{\partial(z,r)}-gw\Theta_0(\psi)=0$$

Defining $\mathcal{H}\equiv\mathcal{H}_0(\psi)+gz\mathcal{H}_1(\psi)$, implies $gw\mathcal{H}_1(\psi)=gw\Theta_0(\psi)$. Therefore, the general solution for $\mathcal{H}$ is

$$\mathcal{H}(\psi)=\mathcal{H}_0(\psi)+gz\Theta_0(\psi)\,.$$

Following Batchelor [15, pp. 543–545], we find from the radial component of the momentum equation:

$$\frac{\partial\mathcal{H}}{\partial r}=v\omega_z-w\omega_\theta$$

where

$$\omega_z=\frac{1}{r}\frac{\partial\Gamma_0}{\partial r}=w\frac{d\Gamma_0}{d\psi}$$

and

$$\omega_\theta=\frac{\partial u}{\partial z}-\frac{\partial w}{\partial r}=-\frac{1}{r}\frac{\partial^2\psi}{\partial z^2}-\frac{\partial}{\partial r}\left(\frac{1}{r}\frac{\partial\psi}{\partial r}\right)\,.$$

Therefore,

$$r\frac{\partial}{\partial r}\left(\frac{1}{r}\frac{\partial\psi}{\partial r}\right)+\frac{\partial^2\psi}{\partial z^2}=r^2\left(\frac{d\mathcal{H}_0}{d\psi}+gz\frac{d\Theta_0}{d\psi}\right)-\Gamma_0\frac{d\Gamma_0}{d\psi}\,. \tag{10}$$

B. Non-Boussinesq Fluid

By a simple transformation, first introduced by Yih [16] for fluids with density or entropy variations, it is possible to generalize the model above to account for large density and temperature variations, i.e., to become a non-Boussinesq model. Define a density-scaled velocity $\mathbf{u}'$ as

$$\mathbf{u}' \equiv \sqrt{\frac{\rho}{\rho_0}}\,\mathbf{u}\,. \tag{11}$$

By virtue of the energy equation (Eq. (3)), and the state equation (Eq. (4)):

$$u\frac{\partial \rho}{\partial r} + w\frac{\partial \rho}{\partial z} = 0$$

The implication is that any function $f(\rho)$ will satisfy the equation $\nabla \cdot (f(\rho)\mathbf{u}) = 0$. Using $f(\rho) = \sqrt{\rho/\rho_0}$ results in

$$\nabla \cdot (\sqrt{\rho/\rho_0}\mathbf{u}) = 0$$

or

$$\nabla \cdot \mathbf{u}' = 0\,. \tag{12}$$

Therefore, the continuity equation is formally the same as that for an incompressible fluid with velocities u', w'.

Consider next the azimuthal momentum equation:

$$w\omega_r - u\omega_z = 0\,.$$

Since the flow is assumed axisymmetric, by the same argument, the azimuthal momentum equation becomes

$$u'\frac{\partial rv'}{\partial r} + w'\frac{\partial rv'}{\partial z} = 0 \tag{13}$$

and is the same as that for an incompressible fluid. Similarly, for the radial and axial momentum equations:

$$\rho_0\left(u'\frac{\partial u'}{\partial r} + w'\frac{\partial u'}{\partial z} - \frac{v'v'}{r}\right) + \frac{\partial p}{\partial r} = 0 \tag{14}$$

$$\rho_0\left(u'\frac{\partial w'}{\partial r} + w'\frac{\partial w'}{\partial z}\right) + \frac{\partial p}{\partial z} + \rho g = 0\,. \tag{15}$$

Therefore, the conservation equations for mass, momentum and energy are formally the same as the Boussinesq equations in the previous section with $\mathbf{u}$ replaced by $\mathbf{u}'$. The only difference now is density and temperature are variables that can significantly vary from their ambient values. Thus, the equation of state can be written as

$$\frac{\rho - \rho_0}{\rho_0} = -\frac{T - T_0}{T} \tag{16}$$

with mass, momentum and energy equations:

$$\nabla \cdot \mathbf{u}' = 0 \tag{17}$$

$$-\mathbf{u}' \times \boldsymbol{\omega}' + \nabla \mathcal{H}' - \left(\frac{T - T_0}{T}\right) \mathbf{g} = 0 \tag{18}$$

$$\mathbf{u}' \cdot \nabla \left(\frac{T}{T_0}\right) = 0\ . \tag{19}$$

Note that the head $\mathcal{H}'$ is defined in terms $\mathbf{u}'$. If we use the same functional forms for H_0, Θ_0, and Γ_0 as in the previous section, we must interpret Θ_0 somewhat differently:

$$\frac{T - T_0}{T} \equiv \Theta_0(\psi)$$

Then, $T/T_0 = 1/[1 - \Theta_0(\psi)]$ and $\rho/\rho_0 = 1 - \Theta_0(\psi)$. Also, the real dimensionless velocities must now be derived from the pseudo velocities $\mathbf{u}'$ as follows:

$$\mathbf{u} = \mathbf{u}' \sqrt{\frac{\rho_0}{\rho}} = \frac{\mathbf{u}'}{\sqrt{1 - \Theta_0(\psi)}}\ . \tag{20}$$

C. Nondimensionalization

Consider an upward vertical flow of gas of "injection" velocity U_i and characteristic normalized temperature differential $\Delta\theta$ along the plane $z = 0$. Let r_0 be the characteristic radial dimension for this source of buoyant flow. Also, assume that the circulation increases with radius, approaching an asymptotic value of Γ_∞. Define a buoyancy velocity $U_0 \equiv \sqrt{2 g r_0 \Delta\theta}$. Then, choose dimensionless variables, denoted by a caret, as follows:

$$\hat{z} = z/r_0, \qquad \hat{r} = r/r_0, \qquad \hat{\psi} = \psi/(\pi r_0^2 U_0), \qquad \hat{p} = p/(\tfrac{1}{2}\rho_0 U_0^2)$$
$$\hat{\mathcal{H}}_0 = \mathcal{H}_0/(\tfrac{1}{2}U_i^2), \qquad \hat{\Theta}_0 = \Theta_0/\Delta\theta, \qquad \hat{\Gamma}_0 = \Gamma_0/\Gamma_\infty\ .$$

The functions $\hat{\mathcal{H}}_0, \hat{\Theta}_0$ and $\hat{\Gamma}_0$ have all been chosen so that they vary between 0 and 1. Note that $\Delta\theta$ is a measure of the deviation of the temperature or density from ambient (or Boussinesq).

Define the swirl number based on the diameter $2r_0$ of the inflow:

$$S = \frac{\Gamma_\infty}{2\pi r_0 U_0} \tag{21}$$

and the ratio of the injection velocity to the buoyancy velocity, which is a Froude number,

$$\epsilon = \frac{U_i}{U_0} = \frac{U_i}{\sqrt{2 g r_0 \Delta\theta}}\ . \tag{22}$$

The swirl number is the reciprocal of the Rossby number Ro defined in the classic paper on fire whirls by Emmons and Ying [1]: hence, $S = 1/Ro$.

Then, the equation for the stream function becomes

$$r\frac{\partial}{\partial r}\left(\frac{1}{r}\frac{\partial \psi}{\partial r}\right)+\frac{\partial^2 \psi}{\partial z^2}=\frac{r^2}{2\pi^2}\left(\epsilon^2\frac{d\mathcal{H}_0}{d\psi}+z\frac{d\Theta_0}{d\psi}\right)-4S^2\Gamma_0\frac{d\Gamma_0}{d\psi} \tag{23}$$

where all variables can now be regarded as dimensionless and the carets denoting dimensionless quantities have been dropped.

D. Asymptotic Approximations

In this study, we have chosen the following forms for $\mathcal{H}_0, \Theta_0$, and Γ_0:

$$\begin{aligned}\mathcal{H}_0(\psi) &= (1-\psi)^2 \\ \Theta_0(\psi) &= (1-\psi)^2 \\ \Gamma_0(\psi) &= 1-\exp[-\psi/(1-\psi)]\,.\end{aligned} \tag{24}$$

Note that the functional forms in Eq. (24) were motivated by the physical scenario considered. For instance, the stream function is the mass flow, and $\mathcal{H}_0(0)$ describes the axial velocity distribution flowing into the domain along the base ($z = 0$). The temperature function is defined so at the origin where the stream function is zero, the temperature is maximum. As the stream function approaches unity, the temperature decays to the reference temperature. Also, when the stream function is zero the circulation is zero, and as the stream function approaches unity, the circulation exponentially asymptotes to the finite value Γ_∞.

We can perform an asymptotic analysis of Eq. (23) for large z. It is convenient to change variables to $\eta = rz^{1/4}$ and expand the stream function $\psi(\eta, z) = \psi_0(\eta) + z^{-1/2}\psi_1(\eta) + ...$ Then, to lead order, $\psi_0 = 1 - e^{-x}$, where $x \equiv \eta^2/(2\pi)$ when $\Theta_0(\psi) = (1-\psi)^2$. Each function has been chosen so that they vary between zero and one. The asymptotic analysis was used to guide the choice of boundary conditions. The boundary conditions that close the formulation of $\psi(r, z)$ are

$$\begin{aligned}&\psi(r,0) = 1-e^{-r^2} \\ &\left.\frac{\partial\psi}{\partial z}\right)_{z\to\infty} = 0 \\ &\psi(0,z) \text{ is bounded} \\ &\psi(r\to\infty, z) = 1\,.\end{aligned} \tag{25}$$

An appropriate initial condition that matches the asymptotic approximations is

$$\psi(r,z) = 1-\frac{\eta^2}{2}e^{-\eta^2/2}\,. \tag{26}$$

To lead order only the swirl parameter enters the analysis. The injection velocity has no effect on the far field: the dynamical balance is between buoyancy and circulation. Moreover, the plume narrows with height, ultimately vanishing in thickness in the (unrealistic) limit as $z \to \infty$.

The stream function equation (Eq. (23)) is solved numerically using the definitions of Eq. (24) and the boundary and initial conditions, Eqs. (25–26). Equation (23) is discretized using second order finite differencing for a standard grid formulation. Note that the form of Eq. (23) is a modified Poisson equation. To facilitate a solution, a pseudotime implicit discretization scheme is implemented. The domain for the calculations has dimensions $4r_0 \times 20r_0$, for the radial and axial directions, respectively. Due to regions of high gradients, especially near the centerline, a fine grid is used for the simulations: 256×1024 cells.

III. Discussion

The equation for the stream function was numerically solved for five swirl numbers, $S = 0.0, 0.5, 1.0, 1.5$ and 2.0, to provide a global picture of the interaction between buoyancy and circulation. The zero value of the swirl number represents the hydrodynamics of the plume in the absence of circulation. The maximum value of the swirl number was chosen to be 2.0. It was found that for swirl numbers greater than 2.0, the low Mach number approximation was invalid because large dynamic pressures relative to ambient pressure occurred. As for the non-Boussinesq model, the ratio of ρ_0/ρ ranged from 1.0 to 4.0, providing a realistic range of temperature ratios that could occur in an experiment.

Contours of the stream function are shown in Fig. 2 for different values of the swirl number. The contour lines significantly bow outward near the base of the plume, and buoyancy is the dominant mechanism for the plume formation. As the swirl number, i.e., the circulation, is increased, the contour lines become more compressed. It is with increasing circulation that the plume begins to constrict radially while stretching vertically. The stream function effects for varying swirl number are also shown in Fig. 3 near the base of the plume at $z = 2.0$. As the circulation is increased, the stream function rapidly increases for smaller and smaller values of radius and the plume width reduces.

Temperature profiles at $z = 2.0$ are shown in Fig. 4(a) for the Boussinesq model ($\rho_0/\rho = 1.0$). The profiles show the shape of the plume when subjected to different values of circulation. The non-swirling flow is very broad near the base of the plume and the temperature profile extends to a radius of 3.0. Once circulation is imparted to the flow, the temperature profiles narrow in width. The non-Boussinesq or "thermally expandable" model ($\rho_0/\rho = 4.0$) shown in Fig. 4(b) emphasizes the large temperature and density gradients. Clearly, the peak temperatures along the centerline increase by a factor of 2.0. Increasing the circulation has the same effect as constricting the radial spread of the plume.

The non-Boussinesq model was also examined for four (4) cases of the thermal expansion parameter ρ_0/ρ. Figure 5 shows a comparison between the temperature profiles for two swirl number cases of 0.0 and 2.0 where ρ_0/ρ varies from 1.0 to 4.0. There are two distinct trends that are discernible: 1.) as the thermal expansion of the plume increases, the overall temperatures within the plume increase, and 2.) increasing the circulation constricts the plume radially.

The axial velocity also plays an important role in the plume development, and emphasizes the straining effects, as seen in Figs. 6(a–b). In the absence of circulation for the Boussinesq model (Fig. 6(a)), the plume has a peak axial velocity that is the same order of magnitude as the characteristic buoyancy velocity U_0. The plume is very broad near the base and the axial velocity extends over several radii. Increased circulation dramatically increases the vertical velocity and constricts it radially. Figure 6(b) shows the effects of circulation for the non-Boussinesq flow. The axial velocities double in magnitude and produce a highly stretched plume. The axial velocity generates strain fields which contribute to the plume stretching.

The trends for the swirl (azimuthal) and radial velocities do not change as dramatically as the axial velocity when the Boussinesq and non-Boussinesq cases are compared. However, the swirl velocity is still a contributor to the plume development. As shown in Figure 7, the swirl velocity peak is offset from the plume nominal centerline, and the velocity decays further out radially. The maximum swirl velocity shifts closer to the centerline with increasing circulation, consistent with the other variables discussed. Furthermore, the azimuthal velocity also increases the straining observed in swirling plumes.

As for the radial velocity, the values are negative and very small (on the order of 0.02). The negative values of radial velocity indicate that fluid is pulled toward the center of the plume to replace fluid displaced upward by the buoyant axial flow. Figures 8(a–b) show that the radial velocity approaches zero at the centerline of the plume and at the maximum radius. For the case of no circulation ($S = 0.0$), there is a gradual monotonic decrease of the radial velocity to a minimum, and then a gradual monotonic increase. Further increasing the swirl number eventually leads to a reduction in the magnitude of the radial velocity, and thus the amount of ambient fluid pulled into the plume.

Figures 9(a–b) are plots of the dynamic pressure normalized by the dynamic reference pressure $\frac{1}{2}\rho_0 U_0^2$. In the swirling buoyant flow, both the axial and the azimuthal velocities become large and more confined to a "core" region near the axis when the swirl number is increased. Such large velocities imply that the dynamic pressure decreases and the normalized pressure becomes a relatively large negative number as seen in these figures. (For reference,

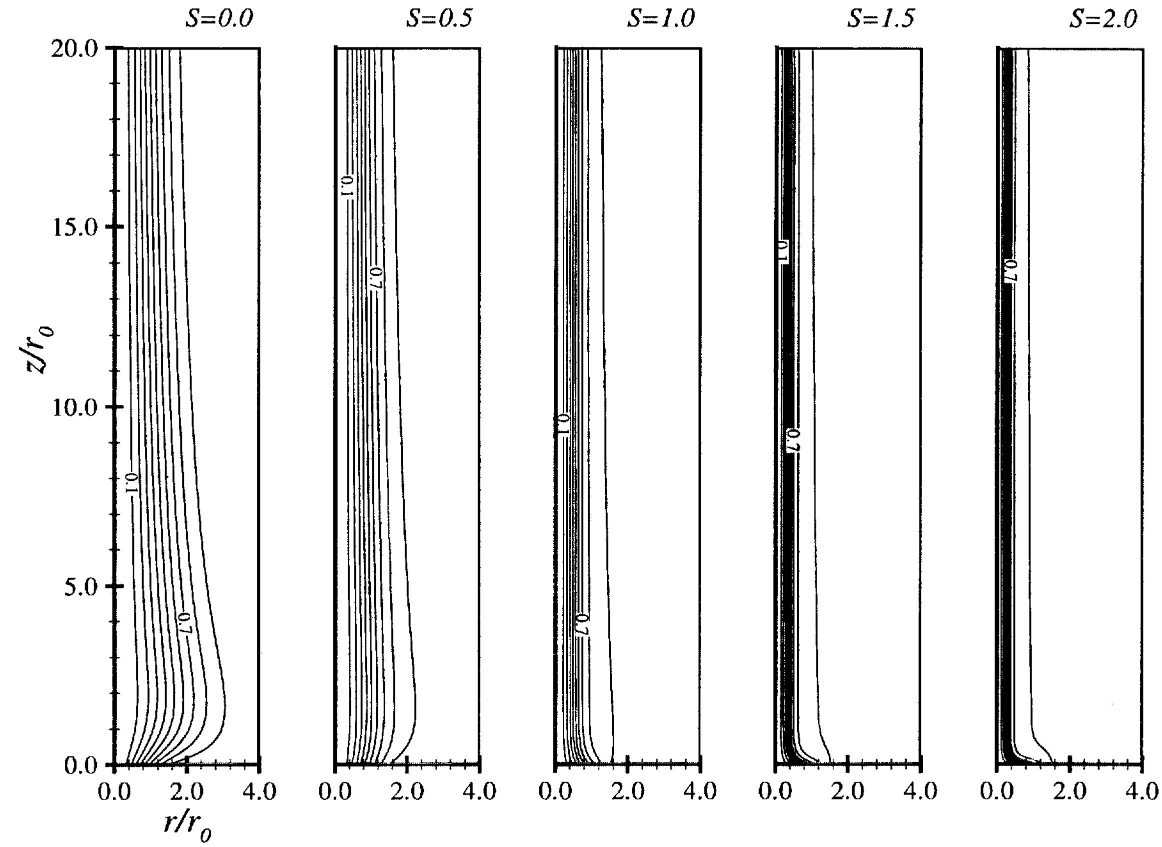

FIGURE 2: Contours of the stream function ψ with swirl number $S = 0.0$ to 2.0.

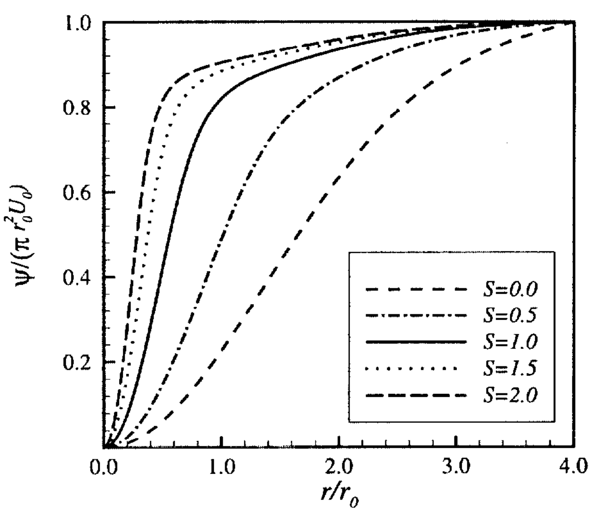

FIGURE 3: Stream function profiles versus radius at $z = 2.0$ with swirl number $S = 0.0$ to 2.0.

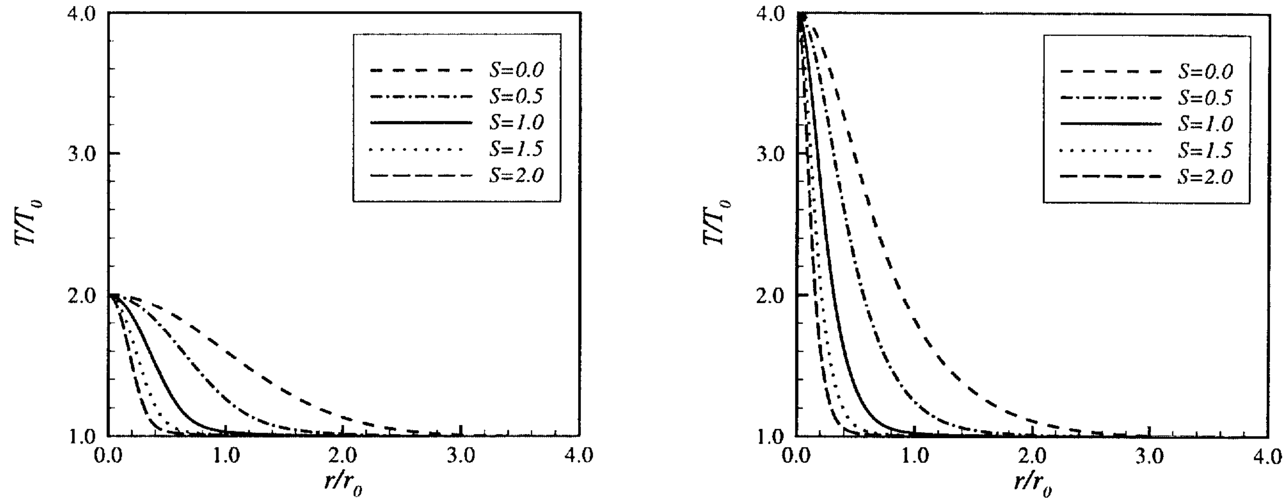

(a) (b)

FIGURE 4: Temperature profiles versus radius at $z = 2.0$ for (a) $\rho_0/\rho = 1.0$ and (b) $\rho_0/\rho = 4.0$.

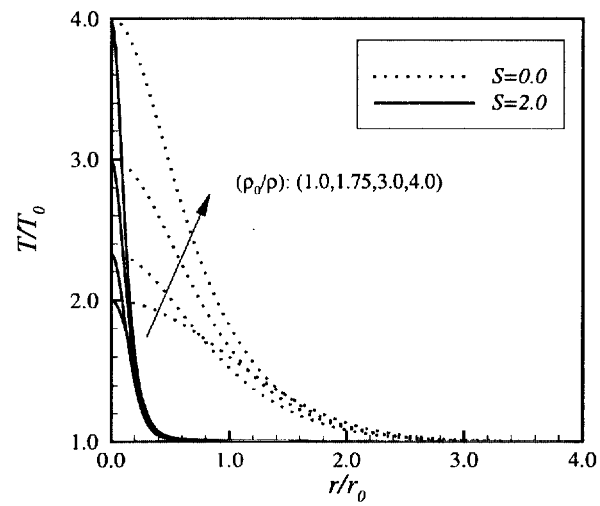

FIGURE 5: Temperature profiles versus radius at $z = 2.0$ with $\rho_0/\rho = 1.0$ to 4.0.

the nondimensional static pressure is about 60,000 so that the total pressure, i.e., static and dynamic, remains positive.) Contrasting Figs. 9(a) and 9(b) shows that the non-Boussinesq model undergoes far greater dynamic pressure deviations with increasing swirl than does the Boussinesq model.

IV. Summary and Conclusions

Motivated by the experiments of Emmons and Ying [1], we have proposed a steady state model of the interaction of circulation with buoyant convection in the absence of mixing or small scale dissipation. While this model introduces many approximations, it also has several valuable features as well. It is tractable, permits the examination of buoyancy, angular-momentum coupling and exhibits many aspects of the results found by the experiments of Emmons and Ying. For example, one of the most interesting but puzzling features of these experiments, as noted already, is the high-aspect-ratio flames that Emmons and Ying could generate. This aspect of swirl-modified buoyant plumes contrasts sharply with other plumes, where the plume is observed to grow radially with increasing axial distance from its source as the buoyant flow entrains surrounding ambient fluid. This entrainment, in turn, increases the volume of axially moving fluid and reduces its axial velocity.

The classical modeling of buoyant plumes starts with the framework established much earlier by Morton et al. [17]. An empirical entrainment coefficient is introduced to account for the ingestion by the plume of ambient fluid and, therefore, its radial growth with distance downstream. This methodology was originally developed for pure momentum-driven jets, and has been extended to account for many other effects in jets and plumes. These models have been enormously successful in the description of buoyant plumes generally and of fire-driven plumes in particular, as well as of jets and jets with buoyancy.

It is natural then, that all modeling of the experiments of Emmons and Ying, including their original model, began with this methodology. Unfortunately, such models have never been able to describe the high-aspect-ratio flames discovered by Emmons and Ying. The model described in this paper can, since the buoyant fluid is constricted by the swirl to rise in a pencil-like flow around the axis of symmetry as shown in Fig. 2 and several following figures. A brilliant aspect of the experiments [1] is that the rotating screen allowed the independent variation of the imposed circulation, a departure from all earlier experiments. An increase of the imposed circulation was found to constrict the radius of the buoyant plume, a feature which is well reproduced in our model; again, see Fig. 2 and subsequent figures. Also, due to the swirl-induced plume constriction and the reduction of entrainment into the plume, all quantities change little with height. Figure 2 also illustrates that the model also shows this behavior.

Another important aspect of our model is that it is not restricted to small density variations. Behavior of the plume for thermally expandable low Mach number flows was also investigated. In a thermally expandable gas, the temperature relative to ambient is inversely related to density relative to ambient. For conditions that would be expected in a fire plume, average temperatures relative to ambient can reach about a factor of four, as shown in Figs. 4 and 5. Swirl confines the radial expansion of the plume just as in the Boussinesq fluid even though the temperature ratios are much higher (and the density ratios correspondingly smaller). Furthermore, due to the larger volume occupied by the high-temperature, low-density gas, the axial velocities are much higher for the thermally expandable gas compared to a Boussinesq gas, as seen by comparison of Figs. 7(a–b).

While the preceding discussion has emphasized the positive comparisons between the experiments of Emmons and Ying and our model, there are also shortcomings of the model. The lack of mixing or of dissipation limits both the possible description of entrainment and also the limitation in height of the high-temperature region (the flame) which physically occurs. These limitations imply that, in the limit of small (or zero) swirl, the model and the experiments will disagree dramatically. In the limit of no swirl, the buoyant plume must grow radially with increasing axial distance from the source as is well known experimentally. However, since there is no mechanism for mixing in the model, entrainment cannot be described, and we find that the plume, while wider than with swirl, remains confined radially with increasing height, much like what one would expect from a laminar buoyant flow. Furthermore, since there is no dissipation in the model, no viscous, thermal conductivity or species diffusion effects, there can be no scale to determine the flame height. Currently, this shortcoming is being investigated.

The model proposed in this paper clearly shows characteristics similar to those found in the pioneering experiments on fire whirls by Emmons and Ying. It is also very different from earlier studies designed to model the interaction of buoyant flow and swirl. As noted earlier, it is very similar both in spirit and in development to that presented in Section 7.4, "Steady axisymmetric flow with swirl," of Batchelor's book [15, pp. 543–545]. That model exhibited unusual and unintuitive characteristics, which, nevertheless could be interpreted physically. For these reasons, we believe that this model deserves both exposition and further study.

References

[1] Emmons, H.W. and S.-J., Ying, The Fire Whirl, *Eleventh Symposium (International) on Combustion*, pp. 475–488 (1967).

[2] Emmons, H.W., Fundamental Problems of the Free Burning Fire, *Tenth Symposium (International) on Combustion*, pp. 951–964 (1965).

[3] Morton, B.R., The Physics of Fire Whirls, *Fire Research Abstracts and Reviews*, **12**(1):1–19 (1970).

[4] Thomas, T.G. and Takhar, H.S., Swirling Motion in a Buoyant Plume, *Acta Mechanica*, **71**:185–193 (1988).

[5] Williams, F.A., Urban and Wildland Fire Phenomenology, *Progress in Energy and Combustion Science*, **8**:317–354 (1982).

[6] Soma, S. and Saito, K., Reconstruction of Fire Whirls Using Scale Models, *Combustion and Flame*, **86**:269–284 (1991).

[7] Hirano, T. and Saito, K., Fire spread phenomena: The role of observation in experiment, *Progress in Energy and Combustion Science*, **20**:461–485 (1994).

[8] Satoh, K. and Yang, K.T., Experimental Observations of Swirling Fires, *ASME HTD*, **335**:393–400 (1996).

[9] Satoh, K. and Yang, K.T., Simulations of Swirling Fires Controlled by Channeled Self-generated Entrainment Flows, *Fire Safety Science – Proceedings of the Fifth International Symposium*, pp. 201–212 (1997).

[10] Chigier, N.A., Beér, J.M., Grecov, D., and Bassindale, K., Jet Flames in Rotating Flow Fields, *Combustion and Flame*, **14**:171–180 (1970).

[11] Tangirala, V. and Driscoll, J.F., Temperature within Non-premixed Flames: Effects of Rapid Mixing Due to Swirl, *Combustion, Science and Technology*, **60**:143–162 (1988).

[12] Gabler, H.C., Yetter, R., and Glassman, I., Asymmetric Whirl Combustion: A New Approach for Non-Premixed Low NOx Gas Turbine Combustor Design, *Proceedings of the 34th AIAA/ASME/SAE/ASEE Joint Propulsion Conference*, AIAA Paper 98-3530, Cleveland, OH, July 1998.

[13] Battaglia, F., McGrattan, K.B., Rehm, R.G., and Baum, H.R., Simulating fire whirls, *Combustion, Theory and Modelling*, (In review, 1999).

[14] Rehm, R.G. and Baum, H.R., The equations of motion for thermally driven, buoyant flows, *Journal of Research, National Bureau of Standards*, **83**(3):297–308 (1978).

[15] Batchelor, G.K., *An Introduction to Fluid Dynamics*, Cambridge University Press, Inc., Cambridge, 1974.

[16] Yih, C.-S., *Dynamics of Nonhomogeneous Fluids*, The MacMillan Company, New York, 1965.

[17] Morton, B.R., Taylor, G.I., and Turner, J.S., Turbulent Gravitational Convection from Maintained and Instantaneous Sources, *Proceedings of the Royal Society*, **A 234**:1–23 (1956).

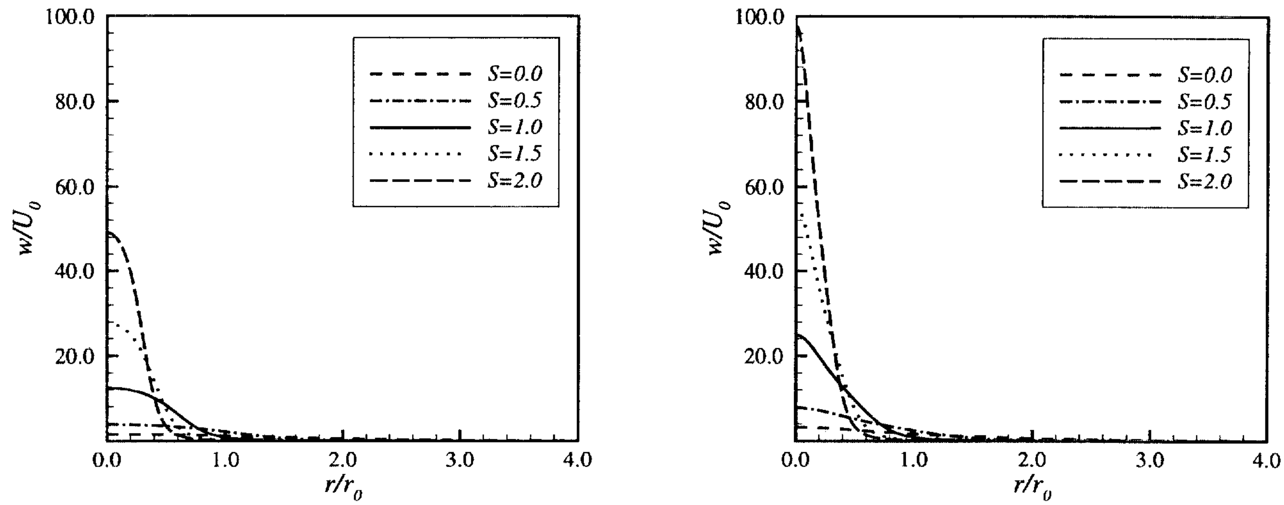

(a) (b)

FIGURE 6: Axial velocity profiles versus radius at $z = 2.0$ for (a) $\rho_0/\rho = 1.0$ and (b) $\rho_0/\rho = 4.0$.

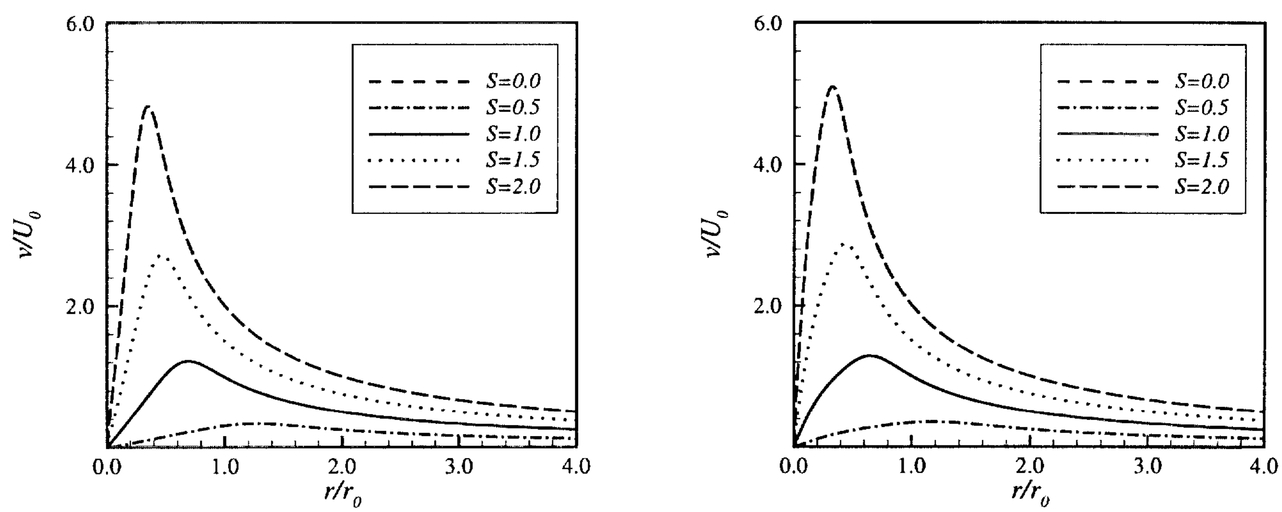

(a) (b)

FIGURE 7: Azimuthal (swirl) velocity profiles versus radius at $z = 2.0$ for (a) $\rho_0/\rho = 1.0$ and (b) $\rho_0/\rho = 4.0$.

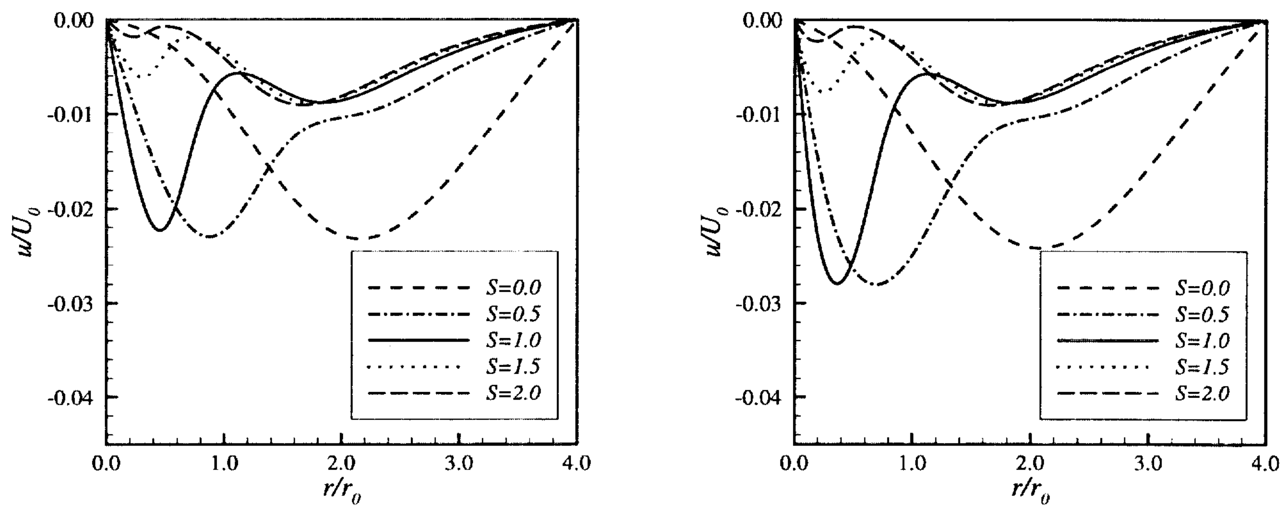

(a) (b)

FIGURE 8: Radial velocity profiles versus radius at $z = 2.0$ for (a) $\rho_0/\rho = 1.0$ and (b) $\rho_0/\rho = 4.0$.

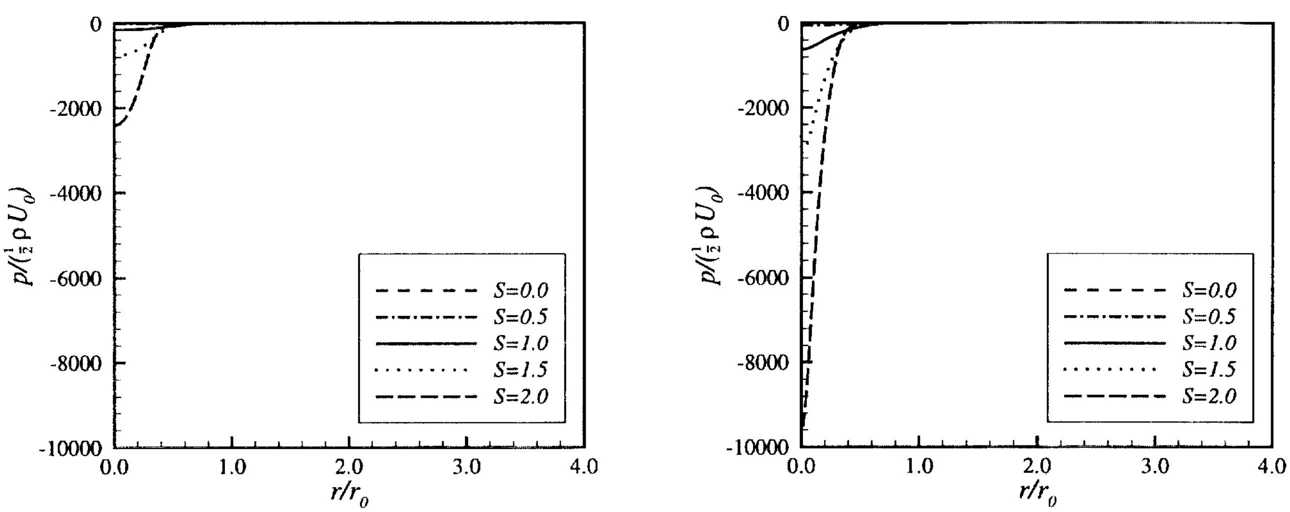

FIGURE 9: Profiles of the pressure coefficient versus radius at $z = 2.0$ for (a) $\rho_0/\rho = 1.0$ and (b) $\rho_0/\rho = 4.0$.